Supplementary Information

S5.1 UCLA LES

The UCLA LES incorporates an interactive radiative transfer computation (Pincus & Stevens, 2009), and a two-moment cloud microphysics parametrization scheme (Seifert & Beheng, 2006) to allow for rain re-evaporation. Surface energy fluxes are described interactively through Monin-Obukhov similarity theory. The latent and sensible heat fluxes entering the atmosphere through the surface thereby vary spatially, increasing at locations of larger surface wind speed. The model uses the Arakawa C-grid and is run at a 200 m horizontal resolution with periodic boundary conditions in the horizontal dimensions. The vertical dimension consists of 75 levels, with a resolution of 100 m below 1 km, gradually increasing to 400 m towards the model top located at 16.5 km. The lower boundary condition, given by surface temperature and humidity is homogeneous across the flat domain. The solar zenith angle is taken as a constant equal to the daily average for tropical insolation (50.5°). Subgrid-scale turbulent fluxes are parametrized according to the Smagorinsky model (Smagorinsky, 1963). Further technical details can be found in the UCLA-LES reference manual (Stevens, 2010).

The equilibrium values of near-surface temperature and humidity were estimated by fitting the exponential $Q(t) = Q_{eq} - Q_0 \cdot \exp(-t/t_0)$ to the convergence towards the equilibrium state (Figure S1). Here Q_{eq} is the equilibrium value, Q_0 the difference $Q_{eq} - Q(t = t_i)$ where t_i is the initial time of the fit, chosen to reduce the impact of spin-up oscillations, and t_0 the inverse rate of approach to the equilibrium state. The initial conditions were chosen as in Haerter and Schlemmer (2018), but are irrelevant for the RCE state. In this state, the imbalance in energy fluxes entering and leaving the system is small, and is not considered to influence the conclusions drawn here.

S5.2 Diagnosing atmospheric stability

Stability within each grid cell of the LES is here considered by computing convective available potential energy (CAPE) and convective inhibition (CIN), defined as

$$\mathrm{CAPE} = g \sum_{z=\mathrm{LFC}}^{\mathrm{LNB}} \frac{T_{\mathrm{vp}} - T_{\mathrm{ve}}}{T_{\mathrm{ve}}} \delta z \tag{S1}$$

$$\mathrm{CIN} = -g \sum_{z=z_0}^{\mathrm{LFC}} \frac{T_{\mathrm{vp}} - T_{\mathrm{ve}}}{T_{\mathrm{ve}}} \delta z, \tag{S2}$$

where g is the acceleration due to gravity, δz the grid spacing in the vertical z-coordinate, and T_{vp} and T_{ve} the virtual temperature of the reference parcel and the environment, respectively. The limits of integration – the level of free convection (LFC) and level of neutral buoyancy (LNB) – are found by first identifying the lifting condensation level (LCL), taken as the level where the vapor pressure of the reference parcel at the level z_0, retaining its water vapor mixing ratio throughout ascent, equals the saturation vapor pressure along the dry adiabat corresponding to the temperature at z_0. Above the LCL, the parcel temperature T_{p} and water vapor mixing ratio q_{p} is found iteratively by computing the moist adiabatic lapse rate Γ_m at every level according to

$$\Gamma_m = g \frac{1 + L_{\mathrm{v}} q_{\mathrm{p}} / R T_{\mathrm{p}}}{c_p + L_{\mathrm{v}}^2 q_{\mathrm{p}} \epsilon / R T_{\mathrm{p}}^2}, \tag{S3}$$

where L_v is the latent heat of vaporization, c_p the specific heat at constant pressure of dry air, R the gas constant for dry air, and ϵ the ratio of the gas constants for dry air and for water vapor. The parcel is assumed to be saturated at every level above the LCL. The resulting parcel virtual temperature profile, by comparison to the ambient virtual temperature profile, yields the grid cell atmospheric stability in terms of CAPE and CIN.

S6 Idealized setup

Haerter et al. (2019) highlights the complexity of interactions between two or three CPs (2CP and 3CP collisions) within the three-dimensional atmosphere. In 2CP collisions, boundary layer air displaced by the outflow boundaries as they collide, can escape either vertically or laterally, whereas in 3CP collisions the resulting outflow is confined to the vertical dimension. Furthermore, in 3CP collisions, the geometry must be such that the air is captured between the colliding outflow boundaries for this to be the case (*see* Figure 3a in Haerter et al. (2019)). Since motion in the channel-like pseudo-2D setup is confined in the narrow dimension, all collisions effectively act like the 3CP collisions in the three dimensional problem, where air must be forced upward. Vertical velocities, and the dynamical effect of CP collisions, can therefore be expected to be overestimated, as lateral escape is never possible. Furthermore, the rapid and inevitable collision of every CP with its own opposite edge in the narrow dimension may decrease the speed of the outflow boundary in the long dimension, due to turbulent kinetic energy generation. Comparing velocities to those in a similar 3D setup shows that horizontal velocities are slightly lower ($\sim$11 % lower on average, Figure S5) and vertical velocities slightly higher in the pseudo-2D setup (Figure S5), in accordance with the above considerations.

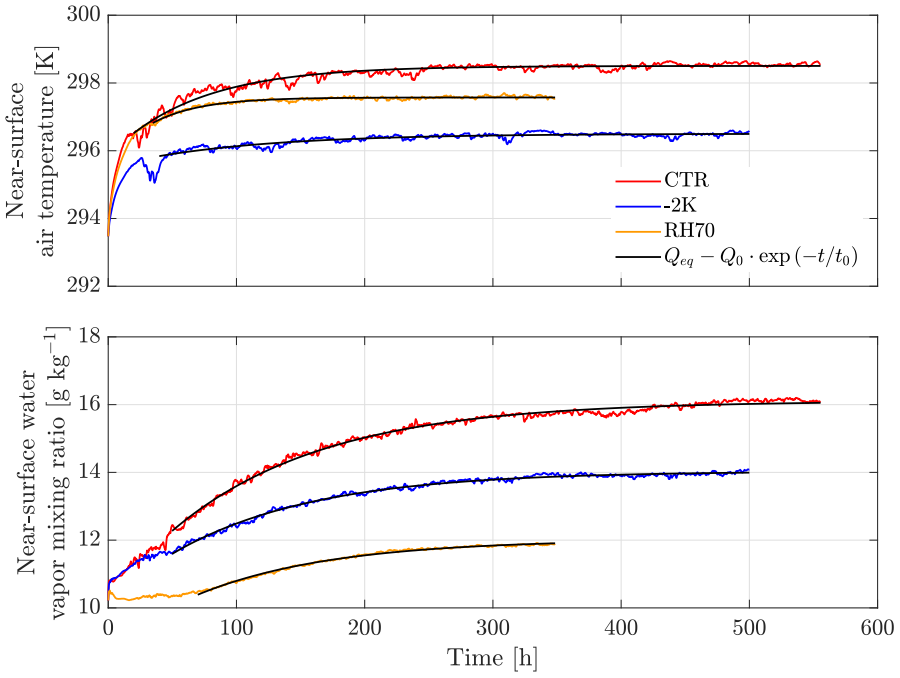

Figure S1. Mean near-surface (50 m) air temperature and water vapor mixing ratio in the three numerical experiments, overlaid by fitted exponential functions.

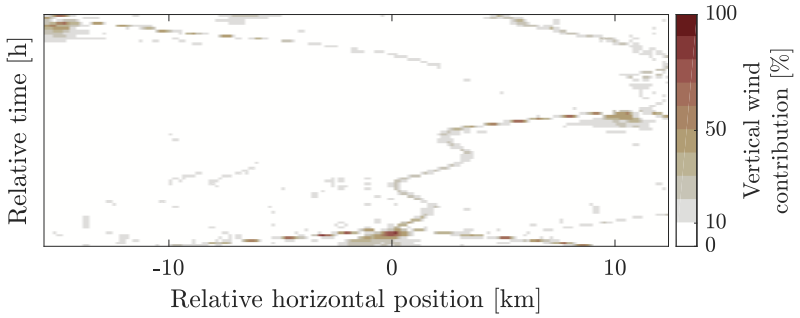

Figure S2. The contribution of vertical wind to the total wind in the area plotted in Figure 3a. The contribution is expressed by the ratio $|w|/\langle\sqrt{v^2+w^2}\rangle \times 100$, of the vertical wind speed $|w|$ to the total velocity averaged over the plotted sub-domain, $\langle\sqrt{v^2+w^2}\rangle$, where v is the horizontal velocity.

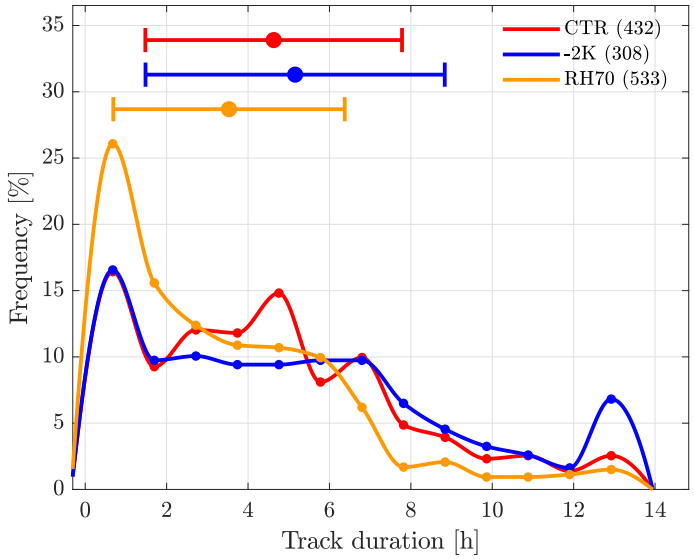

Figure S3. Duration of tracked convergence loci in the three numerical experiments (n given in legend).

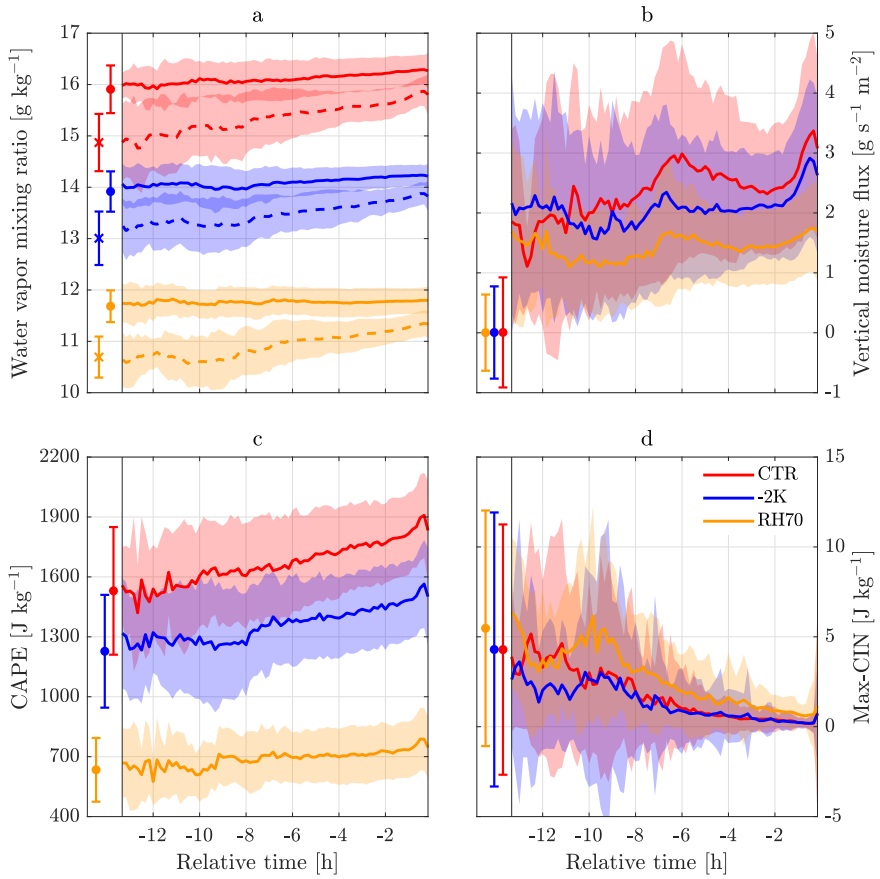

Figure S4. As in Figure 2, but for the full 13.3 h of the aggregate convergence loci.

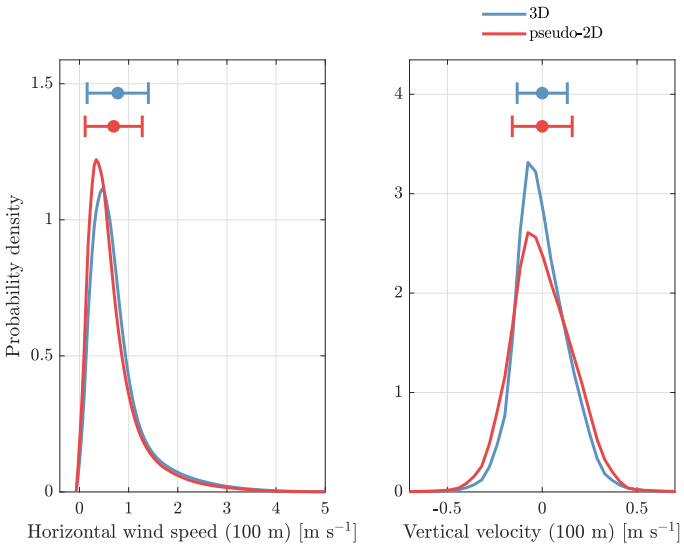

Figure S5. Horizontal and vertical velocities in the pseudo-2D setup (CTR) and in a comparable simulation with horizontal dimensions of equal size (3D). Dots and errorbars show the mean and one standard deviation of the distributions. The 3D simulation is run on the UCLA LES in a 200 km×200 km domain to RCE. The temporal and spatial resolutions (5 min and 400 m, respectively) differ slightly from those used in the 2D setup (10 min and 200 m). The pseudo-2D and 3D simulations are otherwise identical.